ARTICLE

Quantifying Thiol Ligand Density of Self-Assembled Monolayers on Gold Nanoparticles by Inductively Coupled Plasma—Mass Spectrometry

Helmut Hinterwirth,[†] Stefanie Kappel,[‡] Thomas Waitz,[§] Thomas Prohaska,[‡] Wolfgang Lindner,[†] and Michael Lämmerhofer[⊥,*]

[†]Department of Analytical Chemistry, University of Vienna, Währingerstrasse 38, 1090 Vienna, Austria, [‡]Department of Chemistry, Division of Analytical Chemistry-VIRIS Laboratory, University of Natural Resources and Life Sciences (BOKU-UFT), Vienna, Konrad-Lorenz-Straße 24, 3430 Tulln, Austria, [§]Physics of Nanostructured Materials, Faculty of Physics, University of Vienna, Boltzmanngasse 5, 1090 Vienna, Austria, and [⊥]Institute of Pharmaceutical Sciences, University of Tübingen, Auf der Morgenstelle 8, 72076 Tübingen, Germany

ABSTRACT Gold nanoparticles (GNPs) are often used as colloidal carriers in numerous applications owing to their low-cost and size-controlled preparation as well as their straightforward surface functionalization with thiol containing molecules forming self-assembling monolayers (SAM). The quantification of the ligand density of such modified GNPs is technically challenging, yet of utmost importance for quality control in many applications. In this contribution, a new method for the determination of the surface coverage of GNPs with thiol containing ligands is proposed. It makes use of the measurement of the gold-to-sulfur (Au/S) ratio by inductively coupled plasma mass spectrometry (ICP—MS) and its dependence on the nanoparticle diameter. The simultaneous ICP—MS measurement of gold and sulfur was carefully validated and found to be a robust method with a relative standard uncertainty of lower than 10%. A major advantage of this method is the independence from sample preparation; for example, sample loss during the washing steps is not affecting the results. To demonstrate the utility of the straightforward method, GNPs of different diameters were synthesized and derivatized on the surface with bifunctional (lipophilic) ω-mercapto-alkanoic acids and (hydrophilic) mercapto-poly(ethylene glycol) $(PEG)_n$-carboxylic acids, respectively, by self-assembling monolayer (SAM) formation. Thereby, a size-independent but ligand-chain length-dependent ligand density was found. The surface coverage increases from 4.3 to 6.3 molecules nm^{-2} with a decrease of ligand chain length from 3.52 to 0.68 nm. Furthermore, no significant difference between the surface coverage of hydrophilic and lipophilic ligands with approximately the same ligand length was found, indicating that sterical hindrance is of more importance than, for example, intermolecular strand interactions of Van der Waals forces as claimed in other studies.

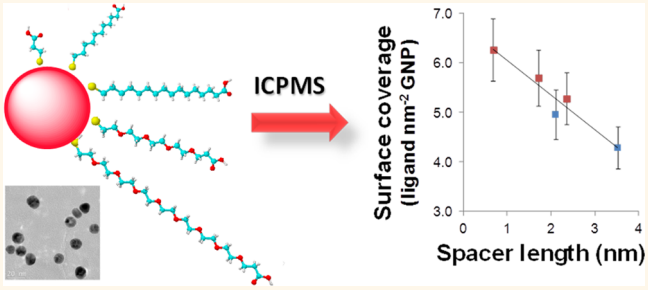

KEYWORDS: inductively coupled plasma mass spectrometry · transmission electron microscopy · surface coverage · self-assembling monolayer

Gold nanoparticles (GNPs) have become popular substrates in nanoscience and nanotechnology for a broad range of biomedical[1−4] and bionanotechnology[5,6] applications as well as for chemical, biological, and clinical diagnostic sensing.[7−14] Besides their unique physical and chemical properties, also their size and size distribution play a key role for their functionality. Therefore, excellent control over properties like size, shape, chemical and colloidal stability, and in particular surface modification of GNPs is crucial in various applications. Thus, tools for their qualitative and quantitative analysis are of extreme importance, not only for quality control in (mass) production but also for health and environmental risk assessment.[15−20]

GNPs can be easily prepared by fast and straightforward size-controlled synthesis through the reduction of $HAuCl_4$. The most frequently utilized method introduced by Frens and Turkevich[21,22] is based on the reduction and simultaneous stabilization with trisodium citrate. In this approach, the size of the nanoparticles can be finely controlled

* Address correspondence to michael.laemmerhofer@uni-tuebingen.de.

Received for review September 7, 2012 and accepted January 20, 2013.

Published online January 21, 2013
10.1021/nn306024a

by the ratio of $HAuCl_4$/reducing agent. Kumar *et al.* described a model for the formation of GNPs that depends on the correlation of citrate/gold ratio and GNP diameter.[23] In this study it is also reported that a stoichiometric ratio larger than 1.5 is needed for complete conversion of auric chloride.

Besides flexible size adjustment, the great popularity of GNPs originates also from their straightforward surface modification by formation of self-assembling monolayers (SAM) with thiol-containing bifunctional ligands.[8,24−26] The bonding of functional ligands exploiting the strong dative bond of sulfur to gold atoms (40−50 kcal mol^{-1} with a strength close to gold−gold bond[27,28]) provides chemically stable functional nanoparticles. This flexible surface functionalization makes this approach technologically attractive.[29]

For many applications, knowledge of the surface coverage of functionalized nanoparticles would be useful, but is seldom reported. Only few papers deal with this issue. X-ray crystallography and density functional theory (DFT) studies have been performed to derive theoretical considerations on the ligand density of thiolate-protected gold complexes ($Au_n(SR)_m$) for small gold clusters with about 1 nm diameter in size (Au_{10}−Au_{144}).[27,30,31] However, gold nanoclusters have due to their ultrasmall size fundamentally different unique properties compared to the larger crystalline GNPs in which the optical properties are dominated by plasmon excitation and possess a collective nature (as opposed to the single-electron transition in gold nanoclusters).[30]

The full-coverage phase, by definition, corresponds to the highest possible packing of the molecules; that is, the surface is saturated. Early studies of the structure of alkanethiols on Au(111) with molecular-level resolution reported diffraction peaks representative of a $(\sqrt{3} \times \sqrt{3})$ R30° structure relative to the underlying Au(111) substrate which corresponds to a molecule−molecule spacing of 5 Å and an area per molecule of 21.6 $Å^2$ (about 4.6 molecules nm^{-2}).[32] Up to now, experimental data on ligand densities, in particular of GNPs defined in the range of 10−100 nm are still rare.[15] Elzey *et al.* reported an average size-independent ligand packing density of 7.8 ± 1.2 nm^{-2} for 5−100 nm gold nanoparticles which were conjugated with 3-mercaptopropionic acid and analyzed by ICP−OES.[33] Packing densities of 4.97 ± 0.01, 4.58 ± 0.01, and 2.20 ± 0.03 ligand molecules nm^{-2} were determined by use of X-ray photoelectron spectroscopy (XPS) for GNPs modified with mercaptoundecanoic acid, mercaptohexanoic acid, and thioctic acid, respectively.[34] Techane *et al.* used XPS for the measurement of the carbon/Au atomic ratio of GNPs with carboxylic acid-terminated alkanethiol monolayers and their characterization dependent of both GNP diameter and alkyl chain length.[35] For a given surface the XPS carbon/Au atomic ratio increased with the chain length owing to the increased number of carbon atoms per molecule. Furthermore, it was shown for a given chain length an increase of the XPS carbon/Au atomic ratio and an increase of the apparent SAM thickness with decrease of GNP size which they explained by the increased curvature of the smaller particles. Lanterna *et al.* determined the degree of surface functionalization based on the shifts of localized surface plasmon resonance spectroscopy (LSPR) as a function of the number of molecules added per nanoparticle.[36] They report a surface density of around 3 molecules nm^{-2} (ranging from 2 to 5 molecules nm^{-2}) for sulfur heterocyclic compounds and described the coverage as almost size-independent. However, they postulated a greater packing density with an increase of the length of the lateral chain changing from 1.2 ± 0.4 to 3 ± 1 molecules nm^{-2} for thiones with a ligand length of 1.2 and 2 nm, respectively. They explained this finding by enforced interstrand Van der Waals (VdW) interactions of ligands with longer chain length. Different labeling assays were explored by Xia *et al.* for quantifying the coverage density of HS-$(PEG)_n$-NH_2 ligands on the surface of gold nanostructures. By this indirect approach they found a decrease of coverage density with an increase of poly(ethylene glycol) (PEG) chain length. Coverage densities of 2.21, 1.33, and 0.21 per nm^2 with the ninhydrin-based assay and of 1.64, 0.85, and 0.14 per nm^2 with fluorescamine-based assay were determined for HS-PEG_{3000}-NH_2, HS-PEG_{5000}-NH_2, and HS-PEG_{20000}-NH_2, respectively.[37] Ratiometric surface-enhanced Raman spectroscopy with an isotope-encoded SERS reference was applied to determine the binding constant and packing density for mercaptobenzimidazole on GNPs *via* measurement of the amount of unbound ligand in the supernatant and fitting of the binding data to the Langmuir isotherm. Saturation capacities of 571 ± 4.6 pmol cm^{-2} were obtained[38] which would be equivalent to about 3.4 ligands per nm^2.

In this paper, we describe a new method for the quantification of the surface coverage of self-assembled thiol ligands bound onto GNPs. This approach is based on the linear correlation between the gold-to-sulfur ratio and the size of SAM-coated GNPs, whereby the ligand density can be calculated from its slope. This method is independent of the nanoparticle concentration, and thus, losses of GNPs during sample preparation, for example, due to adsorption on vessel walls or due to washing steps, will not influence the results. On the other hand, the method needs an accurate determination of the nanoparticle diameter which was analyzed by TEM. Gold nanoparticles with ligands differing in chain length and hydrophilicity/lipophilicity (Table 1) were analyzed by inductively coupled plasma mass spectrometry (ICP−MS). ICP−MS measurements for sulfur in the presence of gold were carefully validated by spiking and recovery experiments.

TABLE 1. Overview of Ligands Used for SAM Modification of GNPs and Their Properties

ligand	abbreviation	formula	MW	ligand length (nm)[a]	log P[b]
3-mercaptopropionic acid	MPA	HS−$(CH_2)_2$−COOH	106.14	0.68	0.43 ± 0.26
11-mercaptoundecanoic acid	MUA	HS−$(CH_2)_{10}$−COOH	218.36	1.71	3.93 ± 0.24
16-mercaptohexadecanoic acid	MHA	HS−$(CH_2)_{15}$−COOH	287.49	2.35	6.58 ± 0.24
SH-PEG4-COOH	PEG_4	HS−$(CH_2CH_2O)_4CH_2CH_2$−COOH	282.11	2.10	−0.66 ± 0.54
SH-PEG7-COOH	PEG_7	HS−$CH_2CH_2(OCH_2CH_2)_7OCH_2CH_2$−COOH	458.57	3.52	−2.09 ± 0.72

[a] The molecular length was determined for a single molecule in vacuum with the most extended chain configuration. Conformations with minimal energy were obtained using the program package Gaussian 03. [b] The values for log P were calculated using ACD/log P DB (ACD/Laboratories, 7.00 Release. Product version 7.07).

The application of ICP−MS for simultaneous measurement of sulfur and gold turned out to be a robust method with relative standard uncertainties lower than 10%.

ICP−MS was demonstrated to be a powerful technique in metal nanoparticle analysis. Along this line, it was recently employed for quantitative analysis of GNPs as well as for size, size distribution, and elemental characterization with and without prior dissolving with aqua regia.[6,39−48] Also the successful hyphenation of chromatographic and electrophoretic techniques with ICP−MS has been realized for characterization of GNPs.[49−53] A combination of laser desorption/ionization and ICP−MS has been recently utilized for the determination of GNP monolayer stability.[54] However, it has not been propagated for surface coverage analysis *via* simultaneous gold to sulfur ratio determination.

RESULTS AND DISCUSSION

Theoretical Calculations. If we assume a set of spherical GNPs saturated with a thiol ligand on the surface, the gold-to-sulfur ratio will depend directly proportionally on the volume-to-surface area ratio. Thus, with increase of diameter D the average number of gold atoms per GNP ($N_{Au/GNP}$) will increase with cube[55]

$$N_{Au/GNP} = \frac{\pi}{6}\frac{\rho D^3}{M_{Au}} \quad (1)$$

while the number of sulfur atoms per GNP ($N_{S/GNP}$) will increase with square and proportionally with the maximal coverage factor k_{max} eq 2.

$$N_{S/GNP} = k\pi D^2 \quad (2)$$

Hence, by combining eqs 1 and 2 it follows that under the assumption of spherical and monodispersed nanoparticles as well as complete saturation of the surface with a monolayer of thiol ligands, the Au/S ratio should increase linearly with the diameter eq 3

$$\frac{N_{Au/GNP}}{N_{S/GNP}} = \frac{\frac{\pi}{6}\frac{\rho D^3}{M_{Au}}}{k_{max}\pi D^2} = k_{max}^{-1} \times 9.83 \times D \quad (3)$$

wherein D is the average diameter of GNPs (in nm), ρ is the density for fcc gold (19.3 g cm^{-3}) and M_{Au} is the atomic weight of gold (196.97 g mol^{-1}) (CAS7440-57-5). Since nanoparticles consist typically as more or less narrow distributions rather than strictly monodisperse particles, Au/S ratios represent also narrow distributions but are experimentally measured as ensemble-averages.

TABLE 2. Calculation of Ligand Coverage As Obtained from the Slope of Au/S Ratios (Measured by ICP−MS) *vs* GNP Size. Given are the Coefficients (Slope and Intercept) of the Linear Regression Function with Standard Errors

ligand	slope	intercept	R^2	coverage (S nm^{-2})
PEG_7	2.32 ± 0.28	−2.3 ± 5.1	0.9595	4.29 ± 0.45
PEG_4	2.00 ± 0.12	−0.3 ± 2.1	0.9903	4.96 ± 0.27
MHA	1.88 ± 0.08	−4.8 ± 1.5	0.9947	5.28 ± 0.21
MUA	1.74 ± 0.04	−0.1 ± 0.7	0.9985	5.70 ± 0.13
MPA	1.59 ± 0.17	−1.7 ± 3.1	0.9683	6.26 ± 0.59

Equation 3 allows the straightforward calculation of the maximum ligand density (i.e., the saturation capacity) k_{max} from the slope of plots of the Au/S ratio *versus* nanoparticle diameter assuming a constant and NP size-independent k_{max}. The validity of this assumption is supported by Supporting Information, Figure S2 which proves a linear dependency and thus a constant slope (statistical parameters see Table 2). If the ligand density would change with nanoparticle diameter, the slope would change with D as well, and this would be materialized by a nonlinear relationship. If the surface coverage for a given ligand is known, the amount of bound ligand per nanoparticle can be easily calculated.

This method has the benefit of being nanoparticle-concentration independent and thus, unaffected by loss of GNPs, for example, during sample preparation and washing steps. Gold and sulfur concentrations and their ratio can be determined simultaneously by ICP−MS and are obtained as ensemble-averages of the particle distributions.

Determination of GNP Diameters, Size Distributions, and Shapes. To establish the correlation of eq 3, GNPs of different sizes were synthesized according to the method by Frens and Turkevich.[21,22] Thus, citrate-capped GNPs were prepared by size-controlled synthesis at variable citrate/$HAuCl_4$ (C/H) ratio between 2 and 6 and analyzed by TEM (Figure 1a).

As expected and reported previously, C/H ratios in the range of 2−6 yield nanoparticles with average sizes between 26.2 ± 4.4 nm and 13.2 ± 1.4 nm in diameter

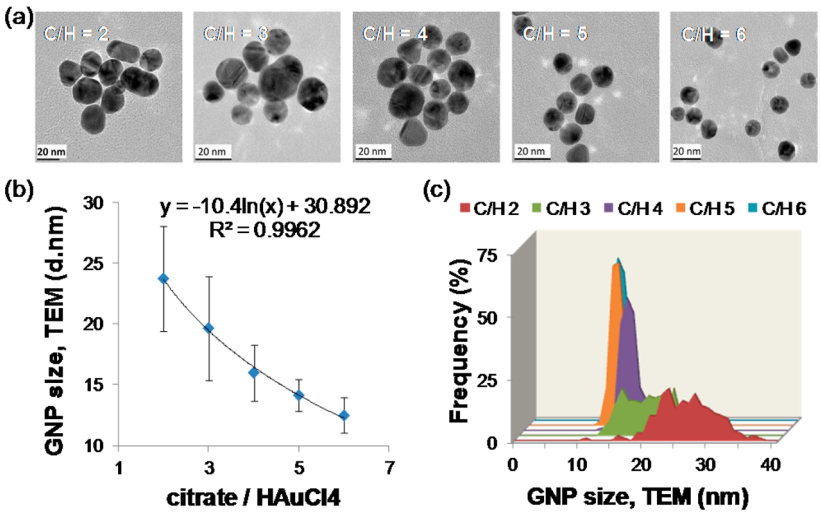

Figure 1. Size and particle size distribution analysis of citrate-capped GNPs by TEM: (a) TEM images of GNPs prepared by different ratios of citrate to $HAuCl_4$ (C/H) from 2 to 6, (b) dependency of GNP diameter on C/H ratio, and (c) polydispersity of GNPs as revealed by corresponding frequency distributions of particle sizes. The trend in panel b can be described by a logarithmic function.

(Figure 1b). GNPs from these batches were used for all further studies. A logarithmic relationship was found between the C/H ratio and the GNP size (Figure 1b), which can be readily utilized in a predictive manner for size-controlled synthesis. Statistical analysis of sufficiently large numbers of particles (>200) in each TEM measurement gives access to information on representative size distributions and morphology. Like in a previous study,[35] it turned out that larger nanoparticles show wider size distributions (Figure 1c) and less uniform spherical shape. Asymmetry factors defined as length-to-width proportion change from 1.21 ± 0.18 for the largest particles to less than 1.09 ± 0.09 for the small GNPs within the specified range of NP diameters.

In a subsequent step, the bifunctional ligands specified in Table 1 were immobilized on the surface of GNPs by formation of SAM coatings. To ensure complete saturation of the GNP surface a large excess of thiol (>10 fold) was used. Finally, the modified GNPs were washed several times to remove excess of unbound ligands.

Determination of Ligand Density. The determination of the ligand coverage *via* the gold-to-sulfur ratio is based on the fact that each ligand on the nanoparticle surface carries a single sulfur atom only while gold atoms constitute the voluminous particle core. Thus, gold increases with cube and sulfur with square of the particle diameter *D*, providing a simple linear relationship between the Au/S ratio and *D*.

For ICP–MS measurements of the Au/S ratio, 2% HCl (v/v) was used for dilution of the samples and preparation of standards. The measured signal intensities were normalized to ^{115}In as internal standard and blank corrected. A prior digestion step before introduction to ICP–MS was not necessary.[42] Quantification was accomplished by external calibration. Furthermore, spike recovery experiments were carried out to validate the sulfur measurement method and to make sure that the presence of gold will not affect the results. In accordance to the work of Jiang *et al.*[44] ICP–MS application for simultaneous measurement of gold and sulfur was found herein to be robust with relative standard uncertainties lower than 10% (for more information see Supporting Information).

The ratio of Au/S as determined by ICP–MS was plotted against the GNP size for the distinctly modified nanoparticles. In fact, for each of the particles linear dependencies as described by eq 3 were observed (see Figure S2 of Supporting Information). Thus, the ligand densities of the fully saturated GNP surfaces could be estimated from the slopes and are summarized in Table 2 along with corresponding data of the regression functions.

It can be seen that the denseness and saturation capacity, respectively, strongly depend on the ligand type (Figure 2a). With an increase of the spacer length, the ligand density dropped significantly from 6.3 molecules nm^{-2} for the short ligand MPA (spacer length = 0.68 nm) to 4.3 molecules nm^{-2} for the longer PEG_7 ligand (spacer length = 3.52 nm) (see Table 2).

This means that for short-chain ligand molecules slightly higher coverages can be achieved experimentally for GNPs as compared to small gold nanoclusters with $(\sqrt{3} \times \sqrt{3})R30°$ structure on Au(111) modified with alkanethiols for which theoretical calculations predicted a maximal upper density limit of ~4.6 molecules nm^{-2}.[26,56] The deviation can be explained by the occupancy of alternative binding sites (edges and corners). This trend of decreasing ligand density for longer-spaced ligands, on the other hand, is largely in agreement with experimentally determined data from Xia *et al.* for long HS-$(PEG)_n$-NH_2 chains.[37]

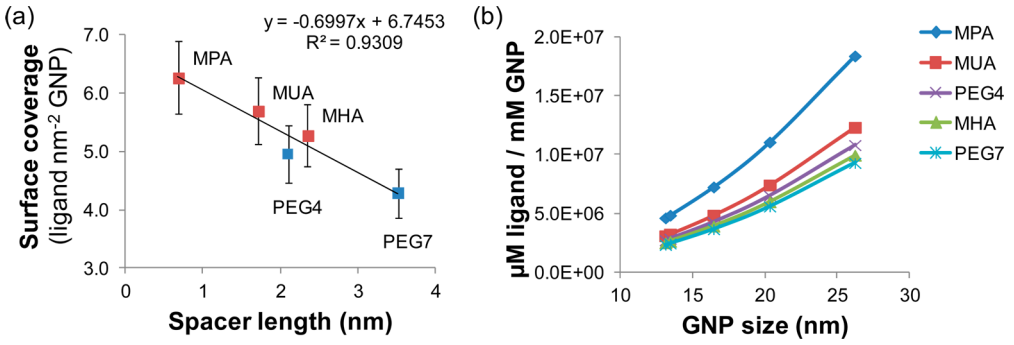

Figure 2. (a) Influence of ligand length on surface coverage (squares, red = mercapto-alkanoic acid, blue = mercapto-$(PEG)_n$-carboxylic acid). (b) Total number of ligands per GNP as calculated from the results of panel a and particle size for the different types of surface modifications.

However, it stands in contradiction to reports of Lanterna *et al*. who measured a slight increase of ligand density with an increase of alkyl chain length of sulfur heterocyclic compounds.[36] This increase with ligand chain length was explained by enforced intermolecular VdW interactions between ligand strands. Stronger VdW interactions with increase of ligand chain-length have also been reported by Techane *et al.*[35] They studied the crystallinity of the SAMs of mercapto-alkanoic acids on flat gold by monitoring the positions of the CH stretching frequencies with FTIR-ATR analysis and described a well-ordered SAM of MHA also on 14 nm GNP. Our experiments revealed that GNPs modified with long chain ligands such as HS-PEG_7-COOH, HS-PEG_4-COOH, and MHA are more stable compared to the short-chain MPA-modified GNPs which could be due to interstrand VdW interactions in long-spaced analogues. Although interstrand VdW interactions may be a plausible reason for high surface coverages with longer alkyl chain ligands, our finding seems also to be reasonable. It may be postulated that sterical hindrance has a significant impact on the maximally achievable saturation capacity. This hypothesis is supported by the fact that no significant difference in surface coverages between the lipophilic MHA and the hydrophilic PEG_4 ligands (log *P* values of 6.58 and −0.66; spacer lengths of 2.35 and 2.10 nm, respectively) was found (ligand density of 5.3 and 5.0 molecules per nm^2, respectively). Stronger VdW interactions and higher surface coverage would be expected for the former if interstrand VdW interactions were the determinant factor for saturation capacities which, however, is not the case. Explanations are on the one hand the increase of the tilt angle with an increase of alkyl chain-length,[57] but also gauche defects and entropic contributions will become increasingly important for longer chains;[32] both contributing to the decreased coverage with an increase of ligand chain-length.

It is evident that the current ICP−MS methodology may be a valuable tool to quantify ligand densities on GNPs. With the maximal surface coverage in hand, one can calculate the average number of ligands attached to the surface of GNPs (Figure 2b) and the actually available ligands per volume of GNP solution (see Supporting Information for a detailed discussion), which is the practically relevant figure in many applications.

TABLE 3. Instrumental Parameters for ICP−QMS (ELAN DRC-e)

RF power/W	1300
nebulizer gas flow/L min^{-1}	0.94
auxiliary gas flow/L min^{-1}	0.7
plasma gas flow/L min^{-1}	15
DRC cell gas	O_2
DRC cell gas flow rate (S, Au, In)/L min^{-1}	0.65
R_{pq} value	
S	0.4
Au	0.45
In	0.4
R_{pa} value	
S	0
Au	0.047
In	0
lens voltage (V)	7.5
analogue stage voltage (V)	−2156
pulse stage voltage (V)	1200
detector	Dual
autolens	ON
isotopes monitored	$^{32}S^{16}O$, $^{34}S^{15}O$, ^{197}Au, ^{115}In
scanning mode	peak hopping
sweeps (reading)	6
readings (replicate)	1
replicates	15
dwell time (ms)	50
integration time (ms)	300

CONCLUSIONS

We present a new method for determination of surface coverage of GNPs based on the linear relationship of the gold/sulfur (Au/S) ratio measured by ICP−MS, and the GNP size, measured by TEM. We found that the ligand density linearly dropped with increasing ligand chain length. The surface densities ranged between 6.3 molecules nm^{-2} for the short ligand MPA (spacer length = 0.68 nm) and 4.3 molecules nm^{-2} for the

longer PEG_7 ligand (spacer length = 3.52 nm). Thereby, no significant difference between lipophilic mercaptoalkanoic acid and hydrophilic mercapto-$(PEG)_4$-carboxylic spacer was observed. It is obvious that the presented method should be equally useful for other metallic nanoparticles such as silver NPs, more so as the determination and analysis of silver nanoparticles with ICP−MS has already been described.[58,59]

METHODS

Chemicals. Gold(III) chloride trihydrate (auric chloride, $HAuCl_4 \times 3H_2O$), trisodium citrate, 16-mercaptohexadecanoic acid (MHA), 11-mercaptoundecanoic acid (MUA), 3-mercaptopropionic acid (MPA), and *O*-(2-carboxyethyl-*O*′-2-mercaptoethyl)heptaethylene glycol (PEG_7) were all obtained from Sigma-Aldrich (Vienna, Austria). Thiol-dPEG_4-acid (PEG_4) was obtained from Celares (Berlin, Germany). HNO_3 (p.a. grade) and the ICP−MS standards (CertiPUR) indium, gold, and sulfur were obtained from Merck KGaA (Darmstadt, Germany). Both, the purified water and the 65% (w/w) HNO_3 p.a. grade underwent one-step and two-step, respectively, sub-boiling in a distillation apparatus (MLS DuoPur, MLS, Leutkirch im Allgäu, Germany) for ICP−MS measurements.

Instruments and Methods. *TEM.* For the TEM analysis, GNPs were deposited on standard support films of amorphous carbon spanning Cu grids. The grids were immersed in the GNP suspension. When the grids were withdrawn, the solution evaporated leaving a high number density of GNPs (typically >100 GNPs μm^{-2}). The Cu grids were transferred to the microscope using a single tilt holder. TEM images were acquired with a Philips CM200 (acceleration voltage 200 kV, equipped with a CompuStage goniometer, a CCD Camera System (Gatan Orius SC600) and a carbon free vacuum system). The point resolution of the microscope is 0.26 nm; previous investigations clearly demonstrated the resolution of Au_{55} clusters (diameter of 1.4 nm) deposited on amorphous carbon films similar to the present study. The magnification at the CCD camera was calibrated using standard calibration line and cross grating replicas with 1200 and 2160 lines mm^{-1} for low and intermediate magnifications, respectively. High magnifications were calibrated using graphitized carbon. This calibration was directly justified by obtaining lattice fringe images of the GNPs that showed a fringe spacing deviating by less than 2% from the spacing of (111) lattice planes. For statistical evaluation 200 particles were analyzed for each sample. Their diameter was determined by the average of length and width as estimation for a spherical model (*i.e.*, by $(l_m + w_m)/2$, where l_m and w_m denote the arithmetic mean of the length and width, respectively).

Inductively Coupled Plasma−Quadrupole Mass Spectrometry. The analyses were accomplished with inductively coupled plasma−quadrupole mass spectrometry (ICP−QMS, ICP−MS) instrument (ELAN DRC-e, PerkinElmer, Waltham, Massachusetts, USA) operated in dynamic reaction cell (DRC) operation mode using O_2 as DRC cell gas. S is measured as $^{32}S^{16}O$ and/or $^{34}S^{16}O$, which enables riddance of the oxygen interference present in the standard operation mode measuring at masses 32 and 34. ^{197}Au and ^{115}In were also measured in DRC mode in order to circumvent a switching between modes.

The DRC cell gas flow rate and the R_{pq} values were optimized prior to the analysis by means of ICP standard solutions of Au (*i.e.*, 10 ng g^{-1}) and S (*i.e.*, 100 ng g^{-1}). Indium was used as the internal normalization standard added to all analyzed solutions with a final In concentration of 1 ng g^{-1}. HCl (2% v/v) was recorded as a blank solution prior to analysis of each individual sample in order to monitor memory effects.

Preliminary studies of GNP samples yielded Au concentrations that were up to 60 times higher than the respective S concentrations (*i.e.*, 83−150 ng g^{-1}). Thus, the R_{pa} value was additionally optimized for Au measurements in order to decrease the Au signal and to avoid overloading of the secondary electron multiplier detector operated in dual mode when measuring S and Au simultaneously in the same solution. The Au signal reaching the detector was reduced to approximately 0.1% of the original signal by applying a R_{pa} value of 0.047. It was shown already by Jiang *et al.* in a validated method that the presence of Au even in high concentrations has a negligible effect on the intensity of $^{32}S^{16}O$ under DRC mode.[44] Operating parameters are given in (Table 3).

All used flasks, test-tubes, and pipet tips were cleaned prior to usage according to a three-step purification procedure: (1) 24 h in a 10% (v/v) HNO_3 bath; (2) 24 h in a 1% (v/v) HNO_3 bath, and (3) rinsing with deionized water. The items were double sealbagged using polyethylene bags.

Dilutions of samples and standard solutions were performed with 2% (v/v) HCl. HCl (2% v/v) was prepared by diluting 37% (m/m) HCl (p.a. grade, Merck KGaA, Darmstadt, Germany) with reagent grade type I water (18.2 MΩ cm at 25 °C, Purelab Classic, Veolia Water Systems Austria GmbH, Vienna, Austria). Both, the reagent grade type I water and the 37% (m/m) HCl were additionally purified by sub-boiling distillation (Savillex Corporation, Eden Prairie, MN, USA, and MLS DuoPur, MLS, Leutkirch im Allgäu, Germany) before use.

The measured signal intensities were normalized to the observed ^{115}In intensity. Blank correction was performed by subtraction of the normalized blank intensity from the normalized signal intensities of the samples and the standard solutions. As 2% (v/v) HCl was recorded as blank solution prior to analysis of each individual sample, each individual sample was blank corrected with its respective blank. The ^{197}Au, $^{32}S^{16}O$ and $^{34}S^{16}O$ concentrations (in ng g^{-1}), respectively, were computed by using the $y = kx + d$ relationships of the linear regressions resulting from the external calibrations. Afterward, the concentrations of ^{197}Au, $^{32}S^{16}O$, and $^{34}S^{16}O$ in mol g^{-1} were calculated by using the atomic weight of Au (196.97 g mol^{-1}) and S (32.06 g mol^{-1}), respectively. Finally, the $^{197}Au/^{32}S^{16}O$ ratios were determined by dividing the ^{197}Au and $^{32}S^{16}O$ concentrations expressed in mol g^{-1}.

Ligand Length Calculations. The molecular length of each ligand was determined for a single molecule in vacuum with the most extended chain configuration. Conformations with minimal energy were obtained using the program package Gaussian 03; log *P* values were calculated using ACD/log *P* DB (ACD/Laboratories, 7.00 Release. Product version 7.07).

Size Controlled Preparation of Citrate-Stabilized GNPs. Gold nanoparticles with different sizes were prepared according to the method described previously.[60] In brief, 50 mL of gold(III) chloride trihydrate solution in bidistilled water (final concentration 1.14 mM) was heated in a clean Erlenmeyer flask under stirring until boiling. All glassware and stirrer were cleaned before use with aqua regia, acetone, and bidistilled water. Under further heating, 5 mL of trisodium citrate (concentration varied depending on the final citrate/$HAuCl_4$ (C/H) ratio in solution; C/H > 2 for complete conversion of $HAuCl_4$[23]) was added and afterward the color changed to brown and red. All chemicals were prepared freshly before use.

Self-Assembling of Thiol Containing Ligands. GNPs were derivatized by the self-assembly of bifunctional thiol containing reagents yielding a carboxylic functionalized surface. Therefore, 100 μL of 7 mM mercapto-alkanoic acid and mercapto-$(PEG)_n$-carboxylic acid, respectively, were added to 1 mL of GNP solution and stirred overnight at ambient temperature. An overview about the ligands employed is given in Table 1. The modified nanoparticles were washed 4× by centrifugation (13 400 rpm, 20 min, MiniSpin, Eppendorf) and resuspended in sub-boiled water.

Conflict of Interest: The authors declare no competing financial interest.

Acknowledgment. Financial support of the "Nano-MALDI" project by the Austrian BMVIT *via* the "Austrian Nano-Initiative" and "MNT-ERA.NET" is gratefully acknowledged. S.K. and T.P.

acknowledge the financial support of the FWF (START FWF267N11). We are grateful to Michal Kohout for DFT calculations.

Supporting Information Available: Additional tables and figures as described in the text. This material is available free of charge *via* the Internet at http://pubs.acs.org.

REFERENCES AND NOTES

1. Dykman, L.; Khlebtsov, N. Gold Nanoparticles in Biomedical Applications: Recent Advances and Perspectives. *Chem. Soc. Rev.* **2012**, *41*, 2256–2282.
2. Dreaden, E. C.; Alkilany, A. M.; Huang, X.; Murphy, C. J.; El-Sayed, M. A. The Golden Age: Gold Nanoparticles for Biomedicine. *Chem. Soc. Rev.* **2012**, *41*, 2740–79.
3. Jiang, X.-M.; Wang, L.-M.; Wang, J.; Chen, C.-Y. Gold Nanomaterials: Preparation, Chemical Modification, Biomedical Applications and Potential Risk Assessment. *Appl. Biochem. Biotechnol.* **2012**, *166*, 1533–1551.
4. Pilolli, R.; Palmisano, F.; Cioffi, N. Gold Nanomaterials as a New Tool for Bioanalytical Applications of Laser Desorption Ionization Mass Spectrometry. *Anal. Bioanal. Chem.* **2012**, *402*, 601–623.
5. Yeh, Y.-C.; Creran, B.; Rotello, V. M. Gold Nanoparticles: Preparation, Properties, and Applications in Bionanotechnology. *Nanoscale* **2012**, *4*, 1871–1880.
6. Scheffer, A.; Engelhard, C.; Sperling, M.; Buscher, W. ICP–MS as a New Tool for the Determination of Gold Nanoparticles in Bioanalytical Applications. *Anal. Bioanal. Chem.* **2008**, *390*, 249–252.
7. Jans, H.; Huo, Q. Gold Nanoparticle-Enabled Biological and Chemical Detection and Analysis. *Chem. Soc. Rev.* **2012**, *41*, 2849–2866.
8. Rana, S.; Bajaj, A.; Mout, R.; Rotello, V. M. Monolayer-Coated Gold Nanoparticles for Delivery Applications. *Adv. Drug Delivery Rev.* **2012**, *64*, 200–216.
9. Lu, F.; Doane, T. L.; Zhu, J.-J.; Burda, C. Gold Nanoparticles for Diagnostic Sensing and Therapy. *Inorg. Chim. Acta* **2012**, *393*, 142–153.
10. Larguinho, M.; Baptista, P. V. Gold and Silver Nanoparticles for Clinical Diagnostics—From Genomics to Proteomics. *J. Proteom.* **2012**, *75*, 2811–2823.
11. Azzazy, H. M. E.; Mansour, M. M. H.; Samir, T. M.; Franco, R. Gold Nanoparticles in the Clinical Laboratory: Principles of Preparation and Applications. *Clin. Chem. Lab. Med.* **2012**, *50*, 193–209.
12. Bedford, E. E.; Spadavecchia, J.; Pradier, C.-M.; Gu, F. X. Surface Plasmon Resonance Biosensors Incorporating Gold Nanoparticles. *Macromol. Biosci.* **2012**, *12*, 724–739.
13. Saha, K.; Agasti, S. S.; Kim, C.; Li, X.; Rotello, V. M. Gold Nanoparticles in Chemical and Biological Sensing. *Chem. Rev.* **2012**, *112*, 2739–2779.
14. Tokonami, S.; Yamamoto, Y.; Shiigi, H.; Nagaoka, T. Synthesis and Bioanalytical Applications of Specific-Shaped Metallic Nanostructures: A Review. *Anal. Chim. Acta* **2012**, *716*, 76–91.
15. European Commission, On the Definition of Nanomaterial (L275). *Off. J. Eur. Union* **2011**, *54*, 38-40.
16. Yu, L.; Andriola, A. Quantitative Gold Nanoparticle Analysis Methods: A Review. *Talanta* **2010**, *82*, 869–875.
17. Lapresta-Fernandez, A.; Fernandez, A.; Blasco, J. Nanoecotoxicity Effects of Engineered Silver and Gold Nanoparticles in Aquatic Organisms. *Trend Anal. Chem.* **2012**, *32*, 40–59.
18. Johnston, H. J.; Hutchison, G.; Christensen, F. M.; Peters, S.; Hankin, S.; Stone, V. A Review of the *in Vivo* and *in Vitro* Toxicity of Silver and Gold Particulates: Particle Attributes and Biological Mechanisms Responsible for the Observed Toxicity. *Crit. Rev. Toxicol.* **2010**, *40*, 328–346.
19. Mueller, R.; Laschober, C.; Szymanski, W. W.; Allmaier, G. Determination of Molecular Weight, Particle Size, and Density of High Number Generation PAMAM Dendrimers Using MALDI-TOF-MS and nES-GEMMA. *Macromolecules* **2007**, *40*, 5599–5605.
20. Harkness, K. M.; Cliffel, D. E.; McLean, J. A. Characterization of Thiolate-Protected Gold Nanoparticles by Mass Spectrometry. *Analyst* **2010**, *135*, 868–874.
21. Turkevich, J.; Stevenson, P. C.; Hillier, J., The Nucleation and Growth Processes in the Synthesis of Colloidal Gold. *Faraday Discuss. Chem. Soc.* **1951**, No. 11, 55-75.
22. Frens, G. Controlled Nucleation for the Regulation of the Particle Size in Monodisperse Gold Supensions. *Nat. Phys. Sci.* **1973**, *241*, 20–22.
23. Kumar, S.; Gandhi, K. S.; Kumar, R. Modeling of Formation of Gold Nanoparticles by Citrate Method. *Ind. Eng. Chem. Res.* **2007**, *46*, 3128–3136.
24. Jadhav, S. A. Functional Self-Assembled Monolayers (SAMs) of Organic Compounds on Gold Nanoparticles. *J. Mater. Chem.* **2012**, *22*, 5894–5899.
25. Pieters, G.; Prins, L. J. Catalytic Self-Assembled Monolayers on Gold Nanoparticles. *New J. Chem.* **2012**, *36*, 1931–1939.
26. Love, J. C.; Estroff, L. A.; Kriebel, J. K.; Nuzzo, R. G.; Whitesides, G. M. Self-Assembled Monolayers of Thiolates on Metals as a Form of Nanotechnology. *Chem. Rev.* **2005**, *105*, 1103–1169.
27. Hakkinen, H. The Gold-Sulfur Interface at the Nanoscale. *Nat. Chem.* **2012**, *4*, 443–55.
28. Pensa, E.; Cortes, E.; Corthey, G.; Carro, P.; Vericat, C.; Fonticelli, M. H.; Benitez, G.; Rubert, A. A.; Salvarezza, R. C. The Chemistry of the Sulfur-Gold Interface: In Search of a Unified Model. *Acc. Chem. Res.* **2012**, *45*, 1183–1192.
29. Ulman, A. Formation and Structure of Self-Assembled Monolayers. *Chem. Rev.* **1996**, *96*, 1533–1554.
30. Jin, R. Quantum Sized, Thiolate-Protected Gold Nanoclusters. *Nanoscale* **2010**, *2*, 343–362.
31. Parker, J. F.; Fields-Zinna, C. A.; Murray, R. W. The Story of a Monodisperse Gold Nanoparticle: Au25L18. *Acc. Chem. Res.* **2010**, *43*, 1289–1296.
32. Schreiber, F. Structure and Growth of Self-Assembling Monolayers. *Prog. Surf. Sci.* **2000**, *65*, 151–256.
33. Elzey, S.; Tsai, D.-H.; Rabb, S. A.; Yu, L. L.; Winchester, M. R.; Hackley, V. A. Quantification of Ligand Packing Density on Gold Nanoparticles Using ICP–OES. *Anal. Bioanal. Chem.* **2012**, *403*, 145–149.
34. Ivanov, M. R.; Haes, A. J. Anionic Functionalized Gold Nanoparticle Continuous Full Filling Separations: Importance of Sample Concentration. *Anal. Chem.* **2012**, *84*, 1320–1326.
35. Techane, S. D.; Gamble, L. J.; Castner, D. G. Multitechnique Characterization of Self-Assembled Carboxylic Acid-Terminated Alkanethiol Monolayers on Nanoparticle and Flat Gold Surfaces. *J. Phys. Chem. C* **2011**, *115*, 9432–9441.
36. Lanterna, A. E.; Coronado, E. A.; Granados, A. M. When Nanoparticle Size and Molecular Geometry Matter: Analyzing the Degree of Surface Functionalization of Gold Nanoparticles with Sulfur Heterocyclic Compounds. *J. Phys. Chem. C* **2012**, *116*, 6520–6529.
37. Xia, X.; Yang, M.; Wang, Y.; Zheng, Y.; Li, Q.; Chen, J.; Xia, Y. Quantifying the Coverage Density of Poly(ethylene glycol) Chains on the Surface of Gold Nanostructures. *ACS Nano* **2012**, *6*, 512–522.
38. Zhang, D.; Ansar, S. M. Ratiometric Surface-Enhanced Raman Quantification of Ligand Adsorption onto a Gold Nanoparticle. *Anal. Chem.* **2010**, *82*, 5910–5914.
39. Helfrich, A.; Bruechert, W.; Bettmer, J. Size Characterisation of Au Nanoparticles by ICP–MS Coupling Techniques. *J Anal. Atom. Spectrom.* **2006**, *21*, 431–434.
40. Hu, S.; Liu, R.; Zhang, S.; Huang, Z.; Xing, Z.; Zhang, X. A New Strategy for Highly Sensitive Immunoassay Based on Single-Particle Mode Detection by Inductively Coupled Plasma Mass Spectrometry. *J. Am. Soc. Mass Spectrom.* **2009**, *20*, 1096–1103.
41. Gillespie, A.; Jao, D.; Andriola, A.; Duda, T.; Yang, C. F.; Yu, L. Gold Nanoparticle Determination by Inductively Coupled Plasma–Mass Spectrometry, Anodic Stripping Voltammetry, and Flame Atomic Absorption Spectrophotometry. *Anal. Lett.* **2012**, *45*, 1310–1320.
42. Allabashi, R.; Stach, W.; Escosura-Muniz, A.; Liste-Calleja, L.; Merkoci, A. ICP–MS: A Powerful Technique for Quantitative Determination of Gold Nanoparticles without Previous Dissolving. *J. Nanopart. Res.* **2009**, *11*, 2003–2011.

43. De Jong, W. H.; Hagens, W. I.; Krystek, P.; Burger, M. C.; Sips, A. J. A. M.; Geertsma, R. E. Particle Size-Dependent Organ Distribution of Gold Nanoparticles after Intravenous Administration. *Biomaterials* **2008**, *29*, 1912–1919.
44. Jiang, W.; Hibbert, D. B.; Moran, G.; Akter, R. Measurement of Gold and Sulfur Mass Fractions in L-Cysteine-Modified Gold Nanoparticles by ICP−DRC−MS after Acid Digestion: Validation and Uncertainty of Results. *J. Anal. Atom. Spectrom.* **2012**, *27*, 1465–1473.
45. Kapellios, E. A.; Pergantis, S. A. Size and Elemental Composition of Nanoparticles Using Ion Mobility Spectrometry with Inductively Coupled Plasma Mass Spectrometry. *J. Anal. Atom Spectrom.* **2012**, *27*, 21–24.
46. Pace, H. E.; Rogers, N. J.; Jarolimek, C.; Coleman, V. A.; Higgins, C. P.; Ranville, J. F. Determining Transport Efficiency for the Purpose of Counting and Sizing Nanoparticles *via* Single Particle Inductively Coupled Plasma Mass Spectrometry. *Anal. Chem.* **2011**, *83*, 9361–9369.
47. Tiede, K.; Boxall, A. B. A.; Tiede, D.; Tear, S. P.; David, H.; Lewis, J. A Robust Size-Characterization Methodology for Studying Nanoparticle Behaviour in Real Environmental Samples, Using Hydrodynamic Chromatography Coupled to ICP−MS. *J. Anal. Atom. Spectrom.* **2009**, *24*, 964–972.
48. Degueldre, C.; Favarger, P. Y.; Wold, S. Gold Colloid Analysis by Inductively Coupled Plasma-Mass Spectrometry in a Single Particle Mode. *Anal. Chim. Acta* **2006**, *555*, 263–268.
49. Hagendorfer, H.; Kaegi, R.; Traber, J.; Mertens, S. F. L.; Scherrers, R.; Ludwig, C.; Ulrich, A. Application of an Asymmetric Flow Field Flow Fractionation Multi-detector Approach for Metallic Engineered Nanoparticle Characterization—Prospects and Limitations Demonstrated on Au Nanoparticles. *Anal. Chim. Acta* **2011**, *706*, 367–378.
50. Helfrich, A.; Bettmer, J. Analysis of Gold Nanoparticles Using ICP−MS-Based Hyphenated and Complementary ESI-MS Techniques. *Int. J. Mass Spectrom.* **2011**, *307*, 92–98.
51. Schmidt, B.; Loeschner, K.; Hadrup, N.; Mortensen, A.; Sloth, J. J.; Bender, K. C.; Larsen, E. H. Quantitative Characterization of Gold Nanoparticles by Field-Flow Fractionation Coupled Online with Light Scattering Detection and Inductively Coupled Plasma Mass Spectrometry. *Anal. Chem.* **2011**, *83*, 2461–2468.
52. Haider, S. R.; Sharp, B. L.; Reid, H. J. On-Line Coupling of Gel Electrophoresis and Inductively Coupled Plasma−Mass Spectrometry. *Trend. Anal. Chem.* **2011**, *30*, 1793–1808.
53. Gray, E. P.; Bruton, T. A.; Higgins, C. P.; Halden, R. U.; Westerhoff, P.; Ranville, J. F. Analysis of Gold Nanoparticle Mixtures: A Comparison of Hydrodynamic Chromatography (HDC) and Asymmetrical Flow Field-Flow Fractionation (AF4) Coupled to ICP−MS. *J. Anal. Atom Spectrom.* **2012**, *27*, 1532–1539.
54. Zhu, Z.-J.; Tang, R.; Yeh, Y.-C.; Miranda, O. R.; Rotello, V. M.; Vachet, R. W. Determination of the Intracellular Stability of Gold Nanoparticle Monolayers Using Mass Spectrometry. *Anal. Chem.* **2012**, *84*, 4321–4326.
55. Liu, X.; Atwater, M.; Wang, J.; Huo, Q. Extinction Coefficient of Gold Nanoparticles with Different Sizes and Different Capping Ligands. *Colloid Surface, B* **2007**, *58*, 3–7.
56. Hostetler, M. J.; Wingate, J. E.; Zhong, C.-J.; Harris, J. E.; Vachet, R. W.; Clark, M. R.; Londono, J. D.; Green, S. J.; Stokes, J. J.; Wignall, G. D.; *et al.* Alkanethiolate Gold Cluster Molecules with Core Diameters from 1.4 to 5.2 Nanometers: Core and Monolayer Properties as a Function of Core Size. *Langmuir* **1998**, *14*, 17–30.
57. Ramin, L.; Jabbarzadeh, A. Odd-Even Effects on the Structure, Stability, and Phase Transition of Alkanethiol Self-Assembled Monolayers. *Langmuir* **2011**, *27*, 9748–9759.
58. Tuoriniemi, J.; Cornelis, G.; Hasselloev, M. Size Discrimination and Detection Capabilities of Single-Particle ICP−MS for Environmental Analysis of Silver Nanoparticles. *Anal. Chem.* **2012**, *84*, 3965–3972.
59. Franze, B.; Strenge, I.; Engelhard, C. Single Particle Inductively Coupled Plasma Mass Spectrometry: Evaluation of Three Different Pneumatic and Piezo-Based Sample Introduction Systems for the Characterization of Silver Nanoparticles. *J. Anal. Atom Spectrom.* **2012**, *27*, 1074–1083.
60. Hinterwirth, H.; Lindner, W.; Laemmerhofer, M. Bioconjugation of Trypsin onto Gold Nanoparticles: Effect of Surface Chemistry on Bioactivity. *Anal. Chim. Acta* **2012**, *733*, 90–97.